INSTITUTE OF PHYSICS PUBLISHING PHYSICS IN MEDICINE AND BIOLOGY

Phys. Med. Biol. **50** (2005) 5983–5995 doi:10.1088/0031-9155/50/24/015

Spherical lesion phantoms for testing the performance of elastography systems

Ernest L Madsen, Gary R Frank, Maritza A Hobson, Hairong Shi, Jingfeng Jiang, Tomy Varghese and Timothy J Hall

Department of Medical Physics, University of Wisconsin, 1300 University Avenue, Room 1530, Madison, WI, USA

E-mail: elmadsen@wisc.edu

Received 15 June 2005, in final form 14 October 2005
Published 7 December 2005
Online at stacks.iop.org/PMB/50/5983

Abstract

A set of three cubic one-litre phantoms containing spherical simulated lesions was produced for use in comparing lesion detection performance of different elastography systems. The materials employed are known to be stable in heterogeneous configurations regarding geometry and elastic contrast ≡ (storage modulus of lesion material) ÷ (storage modulus of background material), and regarding ultrasound and NMR properties. The materials mimic soft tissues in terms of elastic, ultrasound and NMR properties. Each phantom has only one value of elastic contrast (3.3, 4.6 or 5.5) and contains arrays of 1.6 mm, 2 mm, 3 mm and 4 mm diameter spherical simulated lesions. All the spheres of a given diameter are arranged in a regular array with coplanar centres. Elastograms of an array made with ultrasound allow determination of the depth range over which lesions of that diameter and elastic contrast can be detected. Two phantoms are made from agar-plus-gelatin-based materials, and one is made from oil-in-gelatin dispersions. The methods for producing the phantoms are described in detail. Lesion detection performances for two ultrasound systems, both operating at about 7.5 MHz and focused at about 5 cm, were quantified with distinctions between the two systems demonstrated. Neither system was capable of detecting any of the 1.6 mm lesions. Phantoms such as these should be useful in research labs that are refining hardware and/or software for elastography.

1. Introduction

Spherical lesion phantoms for use in testing the performance of *ultrasound* imagers have been reported (Kofler and Madsen 2001). The production methods described there for producing planar arrays of spheres have been adapted to produce the spherical lesion phantoms for elastography which are the subject of this report.

Two types of materials have been developed for producing temporally stable phantoms with inclusions having a Young's modulus that is different from that of the surrounding background (Madsen *et al* 2003, 2005a, 2005b). These materials have been used to produce a set of three phantoms, each containing arrays of spherical inclusions with diameters 1.6, 2, 3 and 4 mm. The elastic contrast has a single value for each phantom, and spheres of each diameter are coplanar and arranged in a regular array. (Elastic contrast equals the ratio of the storage modulus of the inclusion material to the storage modulus of the surrounding background material. The storage modulus is the real part of the complex Young's modulus.) The elastic, ultrasonic and NMR properties simulate soft tissues. The elastic contrasts of the three phantoms are 3.3, 4.6 and 5.5. These values are in the range of elastic contrasts determined for *in vitro* breast tissue specimens. Krouskop *et al* (1998) found, at 1 Hz and 5% pre-compression, that the elastic contrast of invasive and infiltrating ductal carcinoma relative to breast fat was 106 kPa/18 kPa $\approx$ 5.9, while relative to normal glandular tissue was 106 kPa/28 kPa $\approx$ 3.8; the elastic contrast of breast fibrous tissue relative to breast fat was 96 kPa/18 kPa $\approx$ 5.3 and relative to normal glandular tissue was 96 kPa/28 kPa $\approx$ 3.4. The phantom elastic contrasts are also in the range of elastic contrasts in terms of shear storage moduli for 85 Hz shear waves in *in vivo* MR breast elastography (Sinkus *et al* 2005), where elastic contrasts (ratio of shear storage modulus of a lesion to that of the surroundings) vary from about 2 through 5.5.

The primary purpose of this paper is to report the development of a novel type of phantom useful for assessing the performance of elasticity imaging systems. Production techniques are detailed and values of relevant physical parameters are given. The utility of the phantoms is illustrated by comparing the performances of two different ultrasound elastography systems based on simple human observer detectability of the spheres as a function of their diameter, elastic contrast and their distance from the transducer (depth). It is reasonable that the utility of such phantoms—perhaps with larger sphere diameters—could be extended to MR systems.

2. Materials

Two of the phantoms (1 and 2) were formed from mixtures of agar and gelatin, plus additives to adjust ultrasonic and NMR properties and to prevent bacterial invasion. All dry weight concentrations of components are uniform throughout each phantom except for the agar and microscopic glass beads. The latter provide increases in ultrasonic attenuation and backscatter. The greater the dry weight concentration of agar in the spheres relative to that in the background, the higher the elastic contrast. Formalin provides for formaldehyde cross-linking of the gelatin component resulting in thermal stability by raising the melting point to over 60 °C. Preserving is done with Germall-plus® (International Specialty products, Wayne, New Jersey, USA).

The compositions of phantoms 1 and 2 are given in detail in table 1. The method of production of the agar/gelatin materials has been described previously (Madsen *et al* 2005a).

The other type of material, used to make phantom 3, includes dispersions of different concentrations of microscopic oil droplets in a gelatin matrix. Preservation and thermal stability are again accomplished through the presence of Germall-plus® and formalin. However, the Young's modulus is determined by the presence or absence of a dispersion of microscopic safflower oil droplets (Hollywood brand, The Hain Celestial Group, Inc., Melville, New York, USA). The greater the concentration of oil, the lower the storage modulus (real part of the complex Young's modulus). The material forming the spherical inclusions contains no oil droplets, while 50% of the volume of the surrounding background consists of oil droplets. Also, there is a liquid surfactant (liquid Ultra Ivory®, Procter and Gamble

Table 1. Dry-weight per cents of the various components in the agar/gelatin phantoms (1 and 2). The weight per cent of 18 MΩ cm (doubly de-ionized) water is not shown since it just makes up the remainder. The gelatin concentrations in the background and spheres are the same in the agar/gelatin when glass beads are excluded; because of the significant difference in glass bead concentrations between background and spheres, the *weight per cent* of gelatin, e.g., gelatin is higher in the spheres than in the background. The purpose of the $CuCl_2$-$2H_2O$ and EDTA tetra-Na hydrate is to lower the NMR T_1 to tissue-like values, and the purpose of the NaCl is to produce tissue-like coil loading for MR (Rice *et al* 1998).

Material	Agar	Gelatin	$CuCl_2$-$2H_2O$	EDTA tetra-Na hydrate	NaCl	HCHO	Germall plus	Glass bead scatterers
Phantom 1 background	1.17	3.60	0.113	0.33	0.77	0.24	1.45	4.6
Phantom 1 spheres	3.60	3.77	0.119	0.34	0.79	0.25	1.49	0.7
Phantom 2 background	1.11	4.80	0.114	0.33	0.77	0.32	1.45	3.4
Phantom 2 spheres	3.44	4.92	0.116	0.34	0.79	0.33	1.49	0.75

Table 2. Weight per cents of components in the spheres of phantom 3 and in the gel matrix surrounding the microscopic safflower oil droplets when oil is present (background of phantom 3). When oil droplets are present, the volume of liquid surfactant equals approximately 1% of the volume of the gel matrix.

Gelatin	Germall plus	Formalin	Glass beads
12.77	1.24	0.735	0.083

Company, Cincinnati, Ohio, USA) present in the background material having a volume of surfactant equal to 1% of the volume of the matrix gel. The weight per cent of surfactant is not shown in table 2 because it is not known how the surfactant is distributed between the aqueous gel matrix and the oil droplets.

Details of the method of production of these oil-in-gelatin materials have been described elsewhere (Madsen *et al* 2003, 2005b).

To minimize changes in mechanical or geometric properties due to osmotic effects in a heterogeneous phantom such as a spherical lesion phantom, it is important that the composition of the spheres be the same as that of the gel matrix surrounding the microscopic oil droplets in the background material. Table 2 shows the composition of sphere and matrix materials.

3. Phantom geometry and production

All three of the phantoms have the geometry depicted in figures 1 and 2. The geometry is such that each sphere is at least four times its diameter from its nearest neighbour to minimize mechanical cross-talk[1].

The procedure for producing a phantom has four overall steps. First, all spheres are made from a single batch of molten material. Two-part acrylic moulds with opposing equal diameter

[1] The 'rule of thumb' that mechanical cross-talk would be minimized when the distance to the nearest neighbour is at least four times the diameter was suggested to us by Professor Jonathan Ophir of the University of Texas at Houston. Except for 4 mm—or larger—diameter spheres, earlier elastography spherical lesion phantoms made in our lab also had nearest neighbour distances greater than four times the diameter of included spheres.

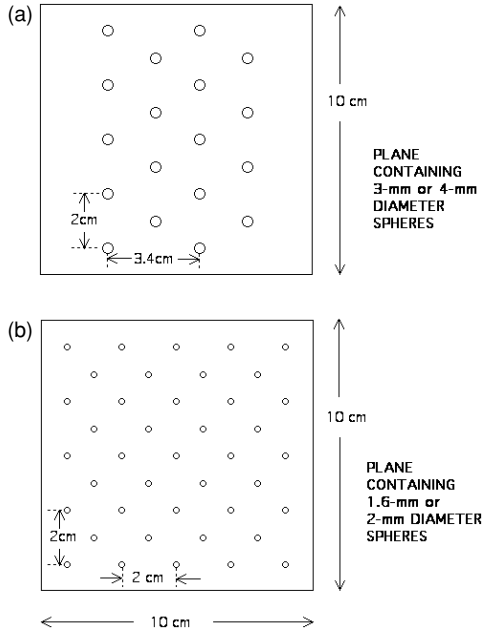

Figure 1. Diagrams showing the planar array of 3 mm and 4 mm diameter spheres (a) and of 1.6 mm and 2 mm diameter spheres in each phantom (b).

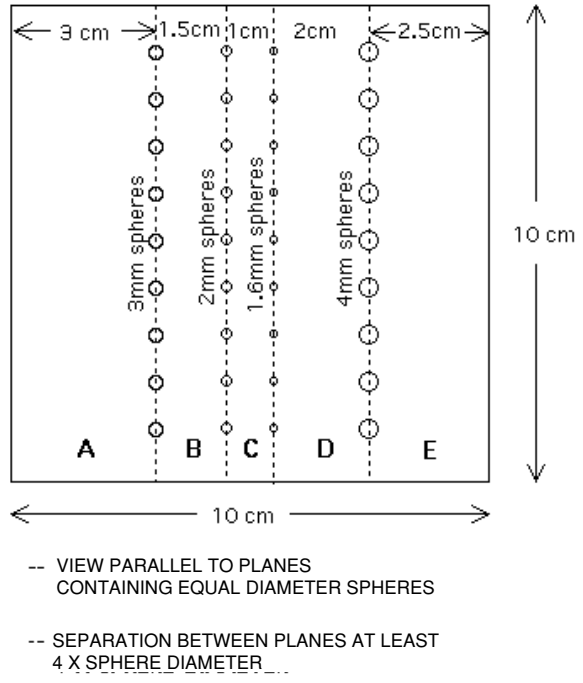

Figure 2. View of phantom with planes containing the centres of equal diameter spheres being perpendicular to the figure. In use, the ultrasound scan planed is superimposed on one of these planes.

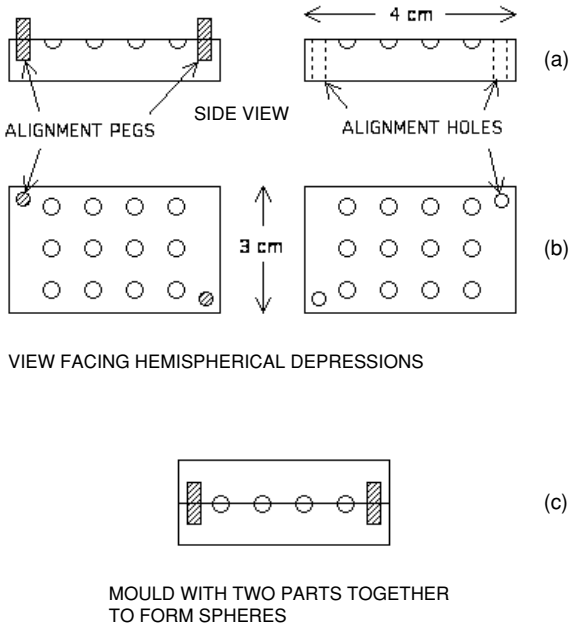

Figure 3. Diagrams of two-part moulds used to form twelve 4 mm diameter spherical inclusions: (a) side view; (b) view facing hemispherical depressions; (c) two parts of the mould pressed together to form 4 mm spheres.

hemispherical depressions are brought together after immersion in the molten material. Prior to immersion, a thin layer of petrolatum is applied to all surfaces to assure release of the spheres from the mould. One part of the mould has two alignment pegs projecting at opposite corners on the same side as the hemispherical depressions. The other side has receiving holes with the same diameter as the pegs. An example of these moulds is shown in figure 3.

The second step is to form sections A and E (figure 2) from one batch of the background material. The same procedure is used to form both sections A and E. The mould components for forming section A are depicted in figure 4. An acrylic plate with 3 mm diameter acrylic hemispheres projecting from one surface is shown in the figure. A frontal view of the plate is shown in figure 4(a) and a side view is shown in figure 4(b). Figure 4(c) shows the mould for forming a 3 cm $\times$ 10 cm $\times$ 10 cm background section of the phantom when the acrylic plate shown in (b) has been clamped onto its open side. The same clamp presses the constraining acrylic plate (d) against the 25 μm thick polyvinylidene chloride film (Saran Wrap®, The Dow Chemical Company, Midland, Michigan, USA) which has been epoxied to the bottom of the 3 cm deep square acrylic rim; the rim defines the lateral boundaries of section A. Acrylic and polyvinylidene chloride film surfaces that will contact the molten background material are coated with a thin layer of petrolatum. The 35 °C molten background material is poured through the filling syringe barrel, and a syringe piston is inserted without trapping air bubbles. (Note that the melting point of the petrolatum is about 45 °C.) A constant force is applied via rubber bands to the piston causing the molten material to be under positive gauge pressure during congealing. Then the clamped unit is rotated at 2 rpm around a horizontal axis until congealing has been completed. The rotation step assures that gravitational sedimentation of background components does not occur.

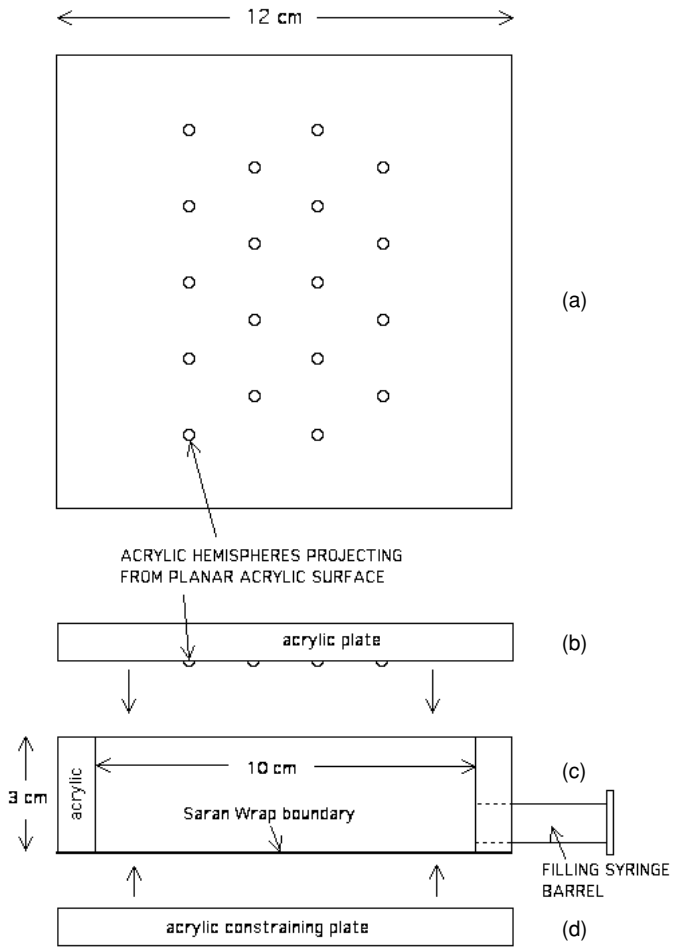

Figure 4. Mould parts for forming background section A (figure 2) of the phantom. A frontal view (a) and side view are shown of an acrylic plate with an array of equal diameter acrylic hemispheres projecting from one surface. A C-clamp is used to clamp that acrylic plate to the second part of the mould (c) along with bottom constraining plate (d) to define section A.

After congealing, the acrylic plate shown in figure 4(b) is removed leaving section A with sockets in the background material into which spherical inclusions can be inserted. To bond a sphere in a socket, a drop of molten background material is placed in the socket followed by immediate insertion of the sphere.

Next, background sections B and D are made in a way equivalent to forming sections A and E except that the polyvinylidene chloride film and constraining plate (figure 4(d)) are missing leaving the bottom of the mould open. The B and D moulds are temporarily glued with 5 min epoxy (Araldite 2012, Huntsman Advanced Materials Americas Inc., East Lansing, Michigan, USA) to the completed sections A and E, respectively. In figure 5 is shown the situation described for section B.

Then a second batch of molten background material is made and sections B and D are filled, the syringe is inserted under positive gauge pressure, and the entire mould system is clamped to a plate rotating at 2 rpm about a horizontal axis to allow congealing without gravitational sedimentation.

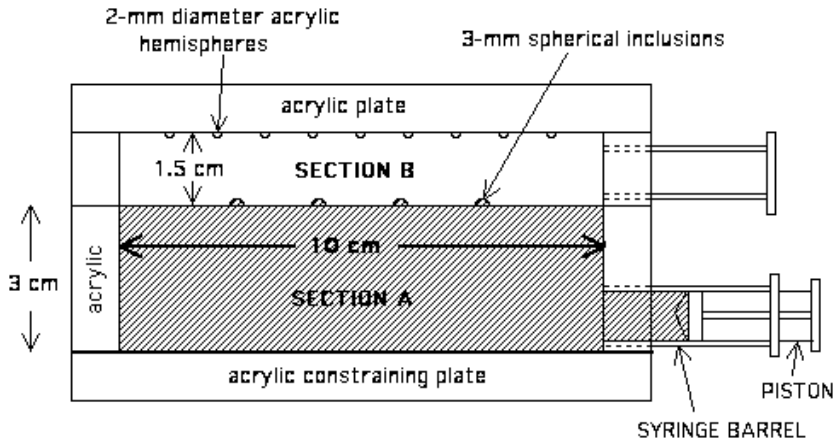

Figure 5. Moulds for production of background section B. Background section A has been completed and the 3 mm diameter spheres have been implanted in its sockets (cross-hatching). The upper bounding acrylic plate has 2 mm diameter acrylic hemispheres projecting downwards to form sockets for the 2 mm diameter spherical inclusions.

Next, the 2 mm and 1.6 mm diameter spheres are glued into their sockets with molten background material and background section C is produced. Sections A + B and D + E, in their respective containers, are 5 min epoxied to a 1 cm thick square acrylic bounding mould with their exposed background surfaces facing one another. Then a third component of molten background material is introduced with 2 rpm rotation, etc.

After about 24 h the completed phantom is removed from its final containing vessel as follows. The polyvinylidene chloride films are removed from sections A and E, and a knife blade is passed around the boundary of the phantom separating it from the acrylic walls and cutting the gel material projecting into the syringe barrels. Then the phantom is slid out of the acrylic walls, submerged in safflower oil in a sufficiently deep container, and the container is covered. The covering of the container will prevent long-term hardening of the safflower oil.

4. Physical properties of the materials

At the time that each batch of molten gel material was made for a phantom, test samples were also produced for determination of storage moduli (real part of the complex Young's modulus), ultrasound propagation speed and attenuation and NMR relaxation times. Regarding determination of storage moduli in a phantom, however, the most reliable method is to employ test samples obtained by excising them from an auxiliary phantom having a cylindrical inclusion made at the same time and of the same materials as those in the spherical lesion phantom (Madsen *et al* 2005a, 2005b). Such cylinder inclusion phantoms were produced in the case of phantoms 2 and 3, but not in the case of phantom 1.

Complete descriptions of the test samples and methods of measurement of properties have been given previously (Madsen *et al* 1999, 2005a). The mechanical, ultrasound and NMR properties of the components of the phantoms are given in tables 3 and 4.

The reason that an auxiliary cylindrical inclusion was not made in the case of phantom 1 is that at the time phantom 1 was made, we did not expect that the elastic contrast found using isolated test samples might be different from that found using excised samples. Following is evidence (not proof) that the value for the elastic contrast of phantom 1 in table 4 is reasonably

Table 3. Mechanical, ultrasound and NMR properties at 22 °C of the materials composing the spheres and backgrounds of the phantoms. Storage moduli for phantom 1 were measured using small samples made at the time the phantom was produced. Storage moduli for phantoms 2 and 3 were measured using test samples excised from cylinder phantoms made at the same time and of the same materials as the corresponding spherical lesion phantom. Storage modulus uncertainties are standard errors (also called standard deviations of the mean) (Bevington 1969) unless a value is less than 3% of the mean; in the latter case the uncertainty is taken to be 3% which is approximately the day-to-day reproducibility for storage modulus determinations. Ultrasound uncertainties are instrumental and NMR relaxation time 'uncertainties' result from curve fitting.

		Ultrasound properties		NMR relaxation times	
Component identity	Storage modulus ± standard error (kPa)	Propagation speed (m s^{-1})	Attenuation coeff. ÷ frequency (dB cm^{-1} MHz^{-1})	T1 (ms)	T2 (ms)
Phantom 1 background	19.6 ± 0.8	1524 ± 1	0.32 ± 0.02	480 ± 1	66 ± 2
Phantom 1 spheres	107.2 ± 3.2	1528 ± 1	0.32 ± 0.02	443 ± 1	45 ± 1
Phantom 2 background	24.4 ± 0.7	1518 ± 1	0.46 ± 0.02	396 ± 1	59 ± 1
Phantom 2 spheres	112.2 ± 3.4	1518 ± 1	0.18 ± 0.02	488 ± 1	53 ± 1
Phantom 3 background	51.0 ± 1.5	1498 ± 1	0.34 ± 0.02	340 ± 20	111 ± 1
Phantom 3 spheres	170 ± 15	1547 ± 1	0.14 ± 0.02	1350 ± 40	290 ± 3

Table 4. Elastic contrasts (storage modulus of inclusion material) ÷ (storage modulus of background material) for the three phantoms using the storage moduli in table 3. Uncertainties are propagated from uncertainties given in table 3.

Phantom 1	Phantom 2	Phantom 3
5.5 ± 0.3	4.6 ± 0.2	3.3 ± 0.3

accurate. One month before production of phantom 1, a cylindrical inclusion phantom was made using the same recipe for inclusion and background as in phantom 1 except that the glass bead concentration in the cylindrical inclusion was eight times that in the spheres of phantom 1. (The glass bead concentration was reduced in the phantom 1 spheres so that the spheres would be more easily detected on B-mode images for alignment purposes.) For the cylindrical inclusion phantom, the elastic contrast determined using isolated test samples differed by only 6% from that using samples excised from the phantom.

5. Apparatus providing for alignment of the ultrasound scan plane on a sphere plane and for precisely controlled axial compressions

To optimize the alignment of the scan plane (plane of symmetry of the scan slice) on one of the planes containing spheres of equal diameter and elastic contrast, the apparatus shown in figure 6 was employed. The phantom is placed on an acoustic absorbing pad in a tank containing safflower oil, the phantom being completely submerged in oil. A constraining plate with a 10 cm × 10 cm square opening is attached to the bottom of the tank, and the base

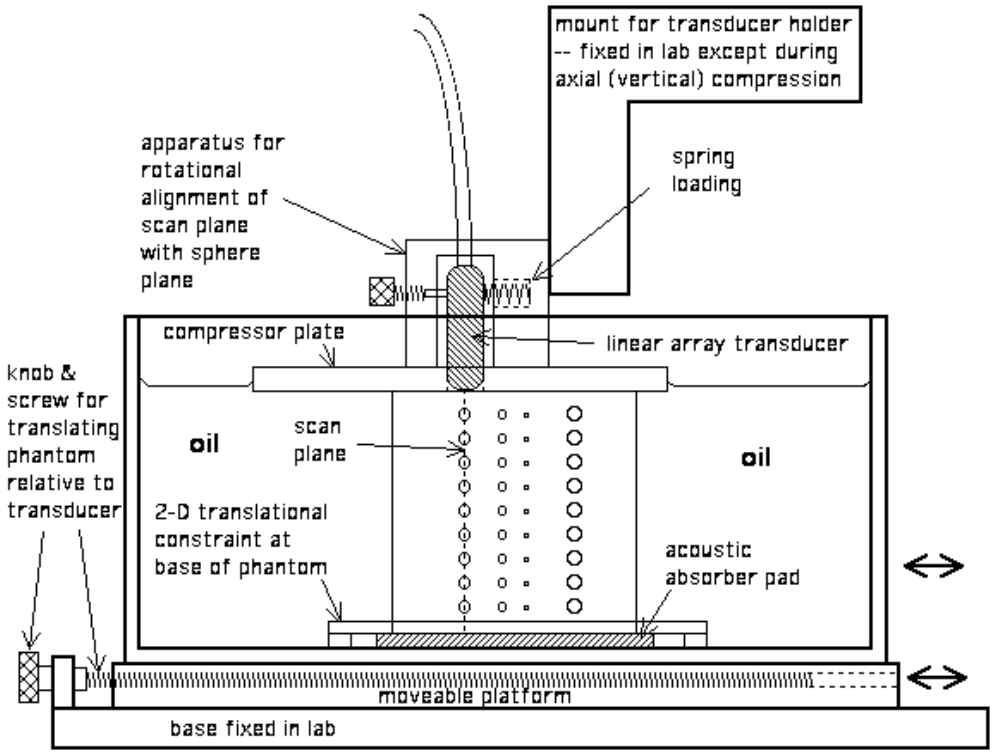

Figure 6. Apparatus used to align the ultrasound scan plane on a plane of spheres with equal diameter and equal elastic contrast and also to allow precisely controlled axial compressions for generating elastograms. See section 5 of the text for a detailed description of its use.

of the phantom is in the square opening, thus fixing the position of the phantom in the tank. Then the transducer is mounted on a single unit for moving the transducer. The transducer fits snugly into a slot in a square 1 cm thick horizontal compression plate and can be rotated about a horizontal axis parallel to the scan plane via a screw and spring-loading apparatus. In the case of the Aloka system, the compression plate was stainless steel with horizontal dimensions 17 cm $\times$ 17 cm; in the case of the Siemens system, the compression plate was acrylic and 13 cm $\times$ 13 cm. The oil tank can be rotated by hand about a vertical axis, and that rotational degree of freedom plus the spring-loaded rotation apparatus allows angular alignment of the scan plane relative to the plane of spheres. Finally, linear translations of the tank (and phantom) can be made perpendicular to the plane of spheres. The two rotations plus the linear translation allow alignment of the scan plane on the plane of spheres. B-mode imaging of the spheres facilitates the alignment. In the case of the 1.6 or 2 mm diameter spheres, they may not be detectable on B-mode images; in that case advantage is taken of the known distances between adjacent sphere planes and the micrometer driven linear translation apparatus.

The two elastography systems existing in our ultrasound laboratory were compared using the phantoms. Both systems employed linear arrays at comparable nominal frequency and focus (Siemens Sonoline Antares with a VFX9–4 array and an Aloka SD 2000 with a 7.5 MHz linear array). Precisely controlled axial compression of the phantom is accomplished by stepper motor or micrometer driven translations of the mount for the transducer holder. In the case of the Aloka system, elastograms were computed from images at 3.9 mm of

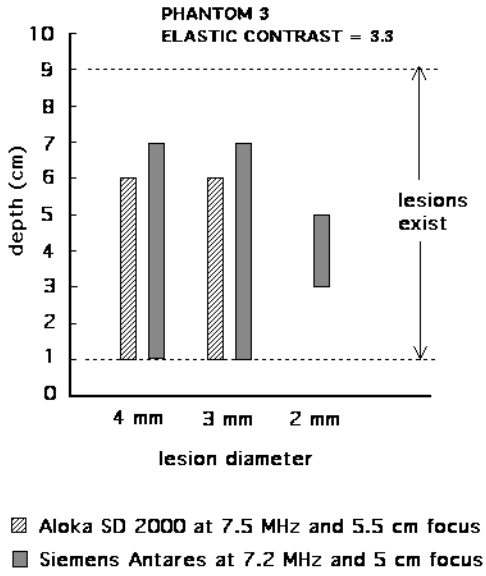

Figure 7. Depth ranges in which spherical lesions were detected on elastograms by human observers using phantom 3 with elastic contrast of 3.3. No evidence of 1.6 mm lesions was present for any scanner. Only the Siemens Antares detected 2 mm lesions. Also, the Siemens system allowed detection of 3 and 4 mm lesions to slightly greater depths than the Aloka system.

compression and 4.35 mm of compression. The corresponding compressions in the case of the Siemens system were 3.0 mm and 4.8 mm.

6. Results and discussion

Results illustrating use of the phantoms for ultrasound elastography are presented in figures 7–9. Depth ranges in which spheres are detectable on elastograms are shown. Note that the highest nominal frequency available for the Aloka system in our lab is 7.5 MHz, and the closest frequency to that available for the Siemens in our lab is 7.2 MHz; thus, these were the frequencies chosen[2]. Two of the coauthors independently determined all depth ranges in which lesions were detectable. The two observers agreed regarding all results shown in the figures.

The Siemens Antares somewhat outperformed the Aloka system for all three phantoms. However, human observers could not detect the 1.6 mm diameter lesions in any of the phantoms, either on B-mode images or on elastograms; this lack of detection is probably due to the fact that the minimum elevational beam full widths at half maximum (FWHM) were comparable to the sphere diameter with corresponding partial volume effects. For the Siemens system, that FWHM was 1.1 mm, and for the Aloka system, it was 1.5 mm. As expected, detection ranges increased with increasing elastic contrast. Note that higher frequency and broader bandwidth transducers available for the Antares (e.g. VFX13-5) may enhance the range of detectability.

Typical models for the variance time delay and displacement estimation applied to motion tracking (Walker and Trahey 1995, Bilgen and Insana 1997) suggest that estimation error is

[2] The Siemens system in our lab can operate at higher frequencies, but we have not yet investigated lesion detection performance for those.

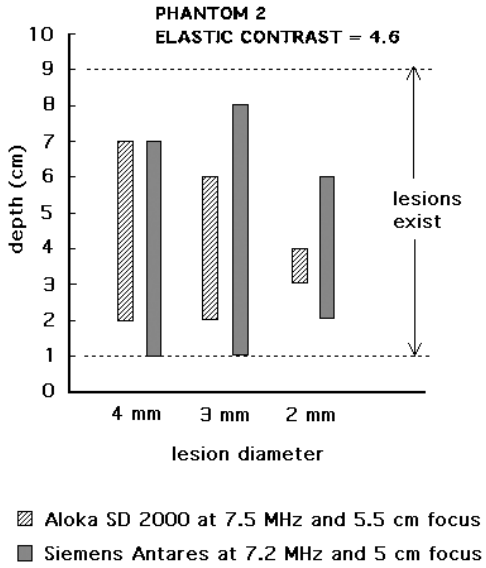

Figure 8. Depth ranges in which spherical lesions were detected on elastograms by human observers using phantom 2 with elastic contrast of 4.6. No detection of 1.6 mm lesions occurred. The Aloka SD 2000 system barely detected 2 mm lesions over a 1 cm depth range. The Siemens system somewhat outperformed the Aloka regarding detection of 3 mm lesions, particularly regarding greater depth of detection.

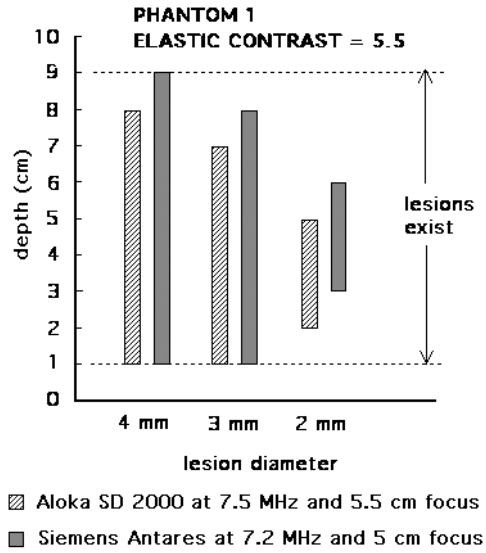

Figure 9. Depth ranges in which spherical lesions were detected on elastograms by human observers using phantom 1 with elastic contrast of 5.5. Again, no detection of 1.6 mm lesions occurred for either system. The Siemens and Aloka systems performed comparably for this phantom which has the highest elastic contrast of the three phantoms. The 4 mm lesions were detected by the Siemens system for the entire depth range where lesions existed, and the Aloka detected the 4 mm lesions over the entire depth except for the most distal cm (8 to 9 cm depth).

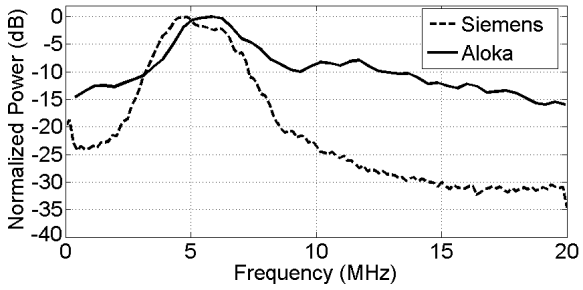

Figure 10. Power spectra of the RF data obtained for the Aloka and Antares system. Both spectra are normalized to their maximum values.

reduced as the radiofrequency (RF) echo signal centre frequency, absolute signal bandwidth and electronic signal-to-noise ratio (SNR) increase. Differences in the performance of the two elasticity imaging systems may partly relate to different estimation errors.

The Siemens Antares Axius Direct Ultrasound Research Interface provides digital signals sampled at 40 MHz and encoded in 16 bits whereas the Aloka system uses external digitization of the RF signals with a GAGE digitization board (Gage Applied Technologies, Inc., Lachine, Quebec, Canada) sampling at 50 MHz and 12 bits. The power spectra of the RF echo data obtained from these systems are shown in figure 10. The power spectra were obtained from Phantom 2 using 1 cm long data segments, centred at 5 cm (approximately their focal depths), from 40 independent A-lines. The centre frequency of the Aloka system (5.2 MHz) is slightly greater than for the Antares (5.0 MHz), while the –6 dB bandwidths obtained using a Gaussian fit are slightly higher for the Aloka (3.4 MHz) than for the Antares (3.2 MHz). The Antares system has a significantly higher signal-to-noise ratio (SNR) at 25 dB compared to the Aloka at 10 dB; the lower SNR of the Aloka may result from external digitization of the RF signals from the Aloka. Note also the presence of a second harmonic in the power spectrum obtained from the Aloka suggesting that the lower SNR for the Aloka is not due to lower transmit pressure.

Another factor that could influence strain image performance involves the method of data processing. A 2D block matching algorithm (Zhu and Hall 2002) was used in the case of the Antares whereas a 1D cross-correlation method was used for the Aloka. The 2D block matching algorithm computes the sum-squared difference (SSD) or sum-absolute difference (SAD) between pre- and post-compression RF frames for a rectangular kernel. The kernel size corresponds to approximately 2/3 the length of the axial point spread function (PSF) and about the same width as the lateral PSF. Linear regression with a sliding 1.5 mm window is used to estimate axial strain from these displacement estimates.

In the 1D cross-correlation method differential displacements in localized regions are detected using standard time-delay estimation techniques (Knapp and Carter 1976, Quazi 1981). A window length of 1.5 mm with a 75% overlap is used to obtain the tissue displacements, and then the axial strain is computed using a 5-point linear least-squares fit on the estimates of tissue displacement (Kallel and Ophir 1997). A 5×5 median filter was used to reduce strain outliers in the strain image.

7. Summary and conclusions

A complete description of the procedure for manufacturing spherical lesion phantoms for elastography with sphere diameters from 1.6 mm through 4 mm has been provided. The

elastic contrasts range from 3.3 through 5.5. Lower elastic contrasts can be produced in the agar/gelatin type phantom by making the dry-weight agar concentration in the spheres closer to that in the background material. Similarly, lower contrasts can be generated in the oil-in-gelatin type phantom by making the spheres from a safflower oil dispersion; the closer the per cent oil in the spheres is to that in the background, the lower the elastic contrast.

It should be noted that the phantoms are durable. About one month after production, bonding between layers of a phantom and between spheres and background is sufficiently firm for at least a 10% compression.

The phantoms brought out differences in performance of the two systems used. A phantom such as described in this work should be useful as a stable performance test tool in labs that are refining hardware and/or software for elastography systems.

Acknowledgments

Work supported in part by NIH grants R01EB000459, R21EB003853 and R01CA100373.

References

Bevington P B 1969 *Data Reduction and Error Analysis for the Physical Sciences* (New York: McGraw-Hill) p 72

Bilgen M and Insana M F 1997 Error analysis in acoustic elastography: I. Displacement estimation *J. Acoust. Soc. Am.* **101** 1139–46

Kallel F and Ophir J 1997 A least-squares strain estimator for elastography *Ultrason. Imaging* **19** 195–208

Knapp C H and Carter G C 1976 The generalized correlation method for estimation of time delay *IEEE Trans. Acoust. Speech Signal Process.* **24** 320–7

Kofler J M Jr and Madsen E L 2001 Improved method for determining resolution zones in ultrasound phantoms with spherical simulated lesions *Ultrasound Med. Biol.* **27** 1667–76

Krouskop T A, Wheeler T M, Kallel F, Garra B S and Hall T J 1998 Elastic moduli of breast and prostate tissues under compression *Ultrason. Imaging* **20** 260–74

Madsen E L *et al* 1999 Interlaboratory comparison of ultrasonic backscatter, attenuation and speed measurements *J. Ultrasound Med.* **18** 615–31

Madsen E L, Frank G R, Krouskop T A, Varghese T, Kallel F and Ophir J 2003 Tissue-mimicking oil-in-gelatin dispersions for use in heterogeneous phantoms *Ultrason. Imaging* **25** 17–38

Madsen E L, Hobson M A, Shi H, Varghese T and Frank G R 2005a Tissue-mimicking agar/gelatin materials for use in heterogeneous elastography phantoms *Phys. Med. Biol.* **50** 5597–5618

Madsen E L, Hobson M A, Shi H, Varghese T and Frank G R 2005b Stability of heterogeneous elastography phantoms made from oil dispersions in aqueous gels *Ultrasound Med. Biol.* at press

Quazi A H 1981 An overview of the time delay estimate in active and passive systems for target localization *IEEE Trans. Acoust. Speech. Signal Process.* **29** 527–33

Rice J R, Milbrandt R H, Madsen E L, Frank G R and Boote E J 1998 Anthropomorphic ^{1}H MRS head phantom *Med. Phys.* **25** 1145–56

Sinkus R, Tanter M, Xydeas T, Catheline S, Bercoff J and Fink M 2005 Viscoelastic shear properties of *in vivo* breast lesions measured by MR elastography *Magn. Reson. Imaging* **23** 159–65 (see figure 5)

Walker W F and Trahey G E 1995 A Fundamental limit on delay estimation using partially correlated speckle signals *IEEE Trans. Ultrason. Ferroelect. Freq. Control* **42** 301–8

Zhu Y and Hall T J 2002 A modified block matching method for real-time freehand strain imaging *Ultrason. Imaging* **24** 161–76